



High-performance LiMn_2O_4 with enwrapped segmented carbon nanotubes as cathode material for energy storage

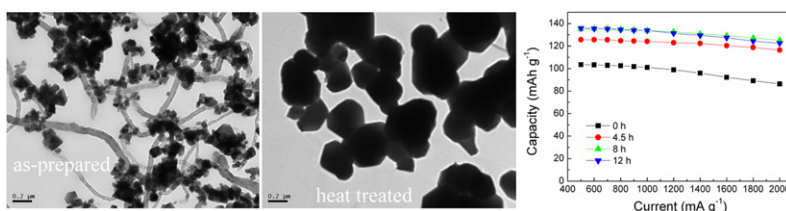
Mengxuan Tang, Anbao Yuan*, Hongbin Zhao, Jiaqiang Xu

Department of Chemistry, College of Sciences, Shanghai University, Shanghai 200444, China

HIGHLIGHTS

- ▶ LiMn_2O_4 with a small amount of enwrapped carbon nanotube (CNT) segments is obtained.
- ▶ This is the first report on LiMn_2O_4 /CNT composite cathode material with this unique architecture.
- ▶ The composite material exhibits excellent high-rate capability in an aqueous electrolyte.
- ▶ Post heat treatment markedly improves the electrochemical performance of the composite.

GRAPHICAL ABSTRACT



ARTICLE INFO

Article history:

Received 7 August 2012
Received in revised form
2 December 2012
Accepted 15 January 2013
Available online 9 February 2013

Keywords:

Spinel lithium manganese oxide
Carbon nanotube
Composite electrode material
Electrochemical performance
Rate capability
Aqueous electrolyte

ABSTRACT

This paper reports a spinel-type LiMn_2O_4 /carbon nanotube (CNT) composite cathode material with high electrochemical performance for energy storage applications. The composite material is prepared by hydrothermal reaction between birnessite MnO_2 /multiwalled carbon nanotube (MWCNT) composite and LiOH solution, followed by heat treatment at 700°C in air atmosphere, where the MnO_2 /MWCNT precursor is obtained by in situ redox reaction between KMnO_4 solution and MWCNTs. The heat treated LiMn_2O_4 /CNT composite material consists of well-crystallized spinel LiMn_2O_4 with small amount of enwrapped segmented carbon nanotubes, which is confirmed by X-ray diffraction and transmission electron microscopy. Electrochemical experimental results demonstrate that the LiMn_2O_4 /CNT composite material heat treated for 8 h exhibits high specific capacity and excellent high-rate capability in 5 M LiNO_3 aqueous electrolyte. The $(\text{LiMn}_2\text{O}_4/\text{CNT})/5\text{ M LiNO}_3/\text{activated carbon}$ hybrid supercapacitor with this LiMn_2O_4 -based composite material as the cathode presents excellent high-power capability and good charge/discharge cyclability.

© 2013 Elsevier B.V. All rights reserved.

1. Introduction

Spinel-type LiMn_2O_4 is a promising cathode material for large-scale high-power rechargeable lithium-ion batteries applied to electric or hybrid electric vehicles and storage of renewable energy, owing to its advantages of abundant manganese resources, low

cost, eco-friendly in nature, high theoretic capacity and facility of production. In the meanwhile, it also suffers the drawback of poor cycling stability. Jahn–Teller effect was believed to be one of the fundamental causes [1]. Some studies have demonstrated that partial substitution of Al^{3+} , Co^{3+} or Cr^{3+} etc, for Mn^{3+} in LiMn_2O_4 could suppress Jahn–Teller distortion to a certain extent, and hence improve the cycling stability of LiMn_2O_4 in nonaqueous organic electrolytes [2–4]. In 1994, Dahn and co-workers reported a lithium-ion battery constructed with a LiMn_2O_4 cathode and a VO_2 (B) anode and 5 M LiNO_3 aqueous solution as the electrolyte [5].

* Corresponding author. Tel.: +86 21 66134851; fax: +86 21 66132797.
E-mail address: abyuan@shu.edu.cn (A. Yuan).

Aqueous lithium-ion batteries have the merits of good safety, low cost and high ionic conductivity of electrolyte. Up to now, several cathode and anode materials such as LiMn_2O_4 [6–27], LiCoO_2 [28–30], LiNiO_2 [31], $\text{Li}[\text{Ni}_{1/3}\text{Co}_{1/3}\text{Mn}_{1/3}]\text{O}_2$ [32], $\text{Li}_x\text{RuO}_{2+0.5x}\cdot n\text{H}_2\text{O}$ [33], LiFePO_4 [34,35], LiV_3O_8 [24,36–38], $\text{LiTi}_2(\text{PO}_4)_3$ [14,39], $\text{VO}_2(\text{B})$ [40] and V_2O_5 xerogel [41] etc, for aqueous lithium-ion batteries or supercapacitors applications have been investigated. Among these materials, the spinel-type LiMn_2O_4 , in general, showed the best performance as a cathode in an aqueous electrolyte, with comparatively better rate charge/discharge capability owing to its three-dimensional tunnel structure for facile diffusion of Li^+ ions and better cycling stability at high charge/discharge current rates, and therefore received the most attention. Studies conducted in our lab have demonstrated that Al^{3+} or Cr^{3+} partial substitution for Mn^{3+} in LiMn_2O_4 could markedly improve its cycling stability in aqueous electrolyte [42,43].

On the other hand, electrode kinetics of LiMn_2O_4 which is related to electron transport in electrode itself and charge transfer at electrode/electrolyte interface is another important concern for operating at high charge and discharge rates when it used as a cathode in high power devices. Hence, LiMn_2O_4 with special morphologies such as ordered mesoporous LiMn_2O_4 , hollow porous LiMn_2O_4 microcubes and double-shelled hollow LiMn_2O_4 microspheres [44–46] and LiMn_2O_4 /conductive carbon composite electrode materials [47–52] attracted much attention in recent years. It has been well demonstrated that LiFePO_4/C composite could be successfully prepared by pyrolysis of an organic carbon precursor in an inert gas [53–55]. Unfortunately, it is difficult to prepare a LiMn_2O_4 /conductive carbon composite material by the above method because LiMn_2O_4 is intrinsically not stable in an oxygen-free atmosphere when it is annealed at a high temperature. Therefore, some other approaches were employed to synthesize LiMn_2O_4 /conductive carbon composite materials. In 2009, a flame spray and a diffusion flame were combined to continuously produce LiMn_2O_4 nanoparticles and carbon black, respectively, to synthesize $\text{LiMn}_2\text{O}_4/\text{C}$ nanocomposites [47]. Also in 2009, a $\text{LiMn}_2\text{O}_4/\text{CNT}$ nanocomposite with nano-sized LiMn_2O_4 dispersed on carbon nanotubes (CNTs) has been synthesized successfully via a microwave-assisted hydrothermal reaction using MnO_2 -coated CNTs and an aqueous LiOH solution [48]. Similarly, a $\text{LiMn}_2\text{O}_4/\text{C}$ composite was synthesized by hydrothermally treating a precursor of manganese oxide/carbon composite in LiOH solution, where the precursor was prepared by reducing potassium permanganate with acetylene black [50]. In 2010, LiMn_2O_4 /multiwalled carbon nanotube (MWCNT) nanocomposites were prepared by a sol–gel method using a unique non-ionic surfactant [51]. In 2011, flexible binder-free $\text{LiMn}_2\text{O}_4/\text{CNT}$ nanocomposites were fabricated by in situ hydrothermal growth [52]. These synthesized LiMn_2O_4 /conductive carbon composites all presented good high-rate capability as cathodes for nonaqueous lithium-ion batteries. In 2009, a $\text{LiMn}_2\text{O}_4/\text{MWCNT}$ composite synthesized by a mechanical activation reaction followed by a heat treatment at 500°C , was used as a cathode for aqueous (1 M Li_2SO_4 solution) lithium-ion battery, and showed better cycling stability and rate capability than the pristine LiMn_2O_4 [49].

We report here a high-performance $\text{LiMn}_2\text{O}_4/\text{CNT}$ composite containing a small amount of enwrapped segmented carbon nanotubes as cathode material for high-power energy storage devices. Firstly, the $\text{MnO}_2/\text{MWCNT}$ composite was obtained by in situ redox reaction between KMnO_4 solution and MWCNTs. Then, the $\text{LiMn}_2\text{O}_4/\text{CNT}$ composite was prepared by a hydrothermal reaction between the $\text{MnO}_2/\text{MWCNT}$ composite and LiOH solution, and finally, the as-synthesized $\text{LiMn}_2\text{O}_4/\text{MWCNT}$ composite was heat treated at 700°C in air atmosphere. The heat treated $\text{LiMn}_2\text{O}_4/\text{CNT}$ composite presented high specific capacity, excellent high-rate capability and good high-rate cycling stability in 5 M LiNO_3

aqueous electrolyte. These performances are much superior to those of the as-synthesized $\text{LiMn}_2\text{O}_4/\text{MWCNT}$ composite and the $\text{LiMn}_2\text{O}_4/\text{AC}$ composite heat treated at the same condition. The influence of heat treatment time on the structure, morphology and electrochemical performance of the $\text{LiMn}_2\text{O}_4/\text{CNT}$ composite material was investigated. We found that heat treatment has a significant effect on improving the performance of the composite material.

2. Experimental

2.1. Materials preparation

As-received multiwalled carbon nanotubes (MWCNTs) were purified by refluxing in 3 M HNO_3 solution at 140°C for 3 h, followed by repeated washing and filtration and then dried at 70°C for 12 h. Given amount of the purified MWCNTs added to a KMnO_4 solution under magnetic stirring. The suspension (mass ratio of $\text{KMnO}_4/\text{MWCNTs} = 8:1$) was adjusted to $\text{pH} \approx 2$ by glacial acetic acid, and then heated to 80°C and kept at this temperature for the in situ redox reaction between KMnO_4 and MWCNTs. After reacting for ca. 3 h, the purple color of the suspension faded out. The clear suspension was repeatedly washed and filtered and then dried at 120°C for 12 h to obtain the MnO_2/CNT composite.

$\text{LiMn}_2\text{O}_4/\text{CNT}$ composite material was prepared by hydrothermal reaction. Given amounts of $\text{LiOH}\cdot\text{H}_2\text{O}$ and the MnO_2/CNT composite (molar ratio of $\text{Li}/\text{Mn} \approx 1:1$) were dispersed in turn into a given amount of distilled water and stirred for ca. 30 min, and then the mixture was transferred to a 50 mL teflon-lined stainless steel autoclave. The autoclave was placed in a drying box to conduct hydrothermal reaction at 180°C for 48 h, and then cooled down naturally to room temperature. The resulting precipitates in the autoclave were rinsed with distilled water and filtered and then dried at 120°C for 12 h.

The as-synthesized $\text{LiMn}_2\text{O}_4/\text{CNT}$ composite material was divided into three parts and heat treated at 700°C in air for 4.5 h, 8 h and 12 h, respectively, to study the influence of heat treatment time on the structure and electrochemical performance of the $\text{LiMn}_2\text{O}_4/\text{CNT}$ composite material.

In addition, a $\text{LiMn}_2\text{O}_4/\text{activated carbon (AC)}$ composite material was also prepared according to the above procedure for comparison with the $\text{LiMn}_2\text{O}_4/\text{CNT}$ composite materials. Firstly, a given amount of KMnO_4 solution reacted with activated carbon (mass ratio of $\text{KMnO}_4/\text{AC} = 4:1$) to obtain MnO_2/AC composite. Then, the MnO_2/AC composite reacted with LiOH solution in an autoclave at 180°C for 48 h to obtain $\text{LiMn}_2\text{O}_4/\text{AC}$ composite, and finally, the as-synthesized $\text{LiMn}_2\text{O}_4/\text{AC}$ composite was heat treated at 700°C in air for 8 h to obtain the heat treated $\text{LiMn}_2\text{O}_4/\text{AC}$ composite.

2.2. Characterization

X-ray diffraction (XRD) analysis was conducted on a Rigaku D/max-2200 X-ray diffractometer with $\text{Cu K}\alpha$ radiation (40 kV/40 mA) at a scan rate of 8°min^{-1} over the 2θ range of 10° – 90° . Morphological observation was performed on a JEOL JEM-200CX transmission electron microscope (TEM). Thermogravimetric and differential thermal analysis (TG–DTA) were carried out on a WCT-1A differential thermal analysis instrument (Beijing, China) at a heating rate of 10°min^{-1} in air. Carbon content was determined using a VARIO EL III elemental analyzer (Elementar Analysensysteme GmbH, Hanau, Germany).

2.3. Fabrication and electrochemical testing of single electrodes

Preparation of working electrodes: $\text{LiMn}_2\text{O}_4/\text{CNT}$ or $\text{LiMn}_2\text{O}_4/\text{AC}$ active material was mixed with acetylene black (AB) and

polytetrafluoroethylene (PTFE) emulsion to form a paste. The paste was coated on a titanium mesh substrate with $1\text{ cm} \times 1\text{ cm}$ area and dried at 105°C , and then roll pressed to a sheet of ca. 0.7 mm thickness, with the mass ratio $\text{LiMn}_2\text{O}_4/\text{CNT}$ (or $\text{LiMn}_2\text{O}_4/\text{AC}$):AB:PTFE = 75:20:5. Preparation of counter electrode: commercial activated carbon (AC) was mixed with AB and PTFE emulsion to form a paste. The paste was coated into a nickel foam substrate with $2\text{ cm} \times 2\text{ cm}$ area and dried at 105°C , and then roll pressed to ca. 1.0 mm thickness. The mass ratio of the formed electrode is AC:AB:PTFE = 78:14:8. Electrochemical experiments were conducted using a three-electrode glass cell with $\text{LiMn}_2\text{O}_4/\text{CNT}$ (or $\text{LiMn}_2\text{O}_4/\text{AC}$) working electrode and AC counter electrode immersed in 5 M LiNO_3 aqueous electrolyte, and saturated calomel electrode (SCE) as reference electrode. Cyclic voltammetric measurement was carried out on a Solartron Model 1287 instrument. Galvanostatic charge/discharge test was conducted on a LAND CT2001A autocyler (Wuhan, China) at 30°C .

2.4. Fabrication and charge/discharge testing of $(\text{LiMn}_2\text{O}_4/\text{CNT})//\text{AC}$ hybrid supercapacitor

Fabrication of $(\text{LiMn}_2\text{O}_4/\text{CNT})//\text{AC}$ hybrid supercapacitor: the $\text{LiMn}_2\text{O}_4/\text{CNT}$ positive electrode was fabricated using the $\text{LiMn}_2\text{O}_4/\text{CNT}$ composite active material heat treated at 700°C for 8 h , and the AC negative electrode was fabricated using the commercial activated carbon powder as the active material. The mass loading of the positive electrode and the negative electrode active materials follows the mass ratio $\text{LiMn}_2\text{O}_4/\text{CNT}:\text{AC} = 1:3$. A piece of polypropylene separator was sandwiched between the $\text{LiMn}_2\text{O}_4/\text{CNT}$ positive electrode and the AC negative electrode, and then placed into 5 M LiNO_3 aqueous electrolyte solution to construct a $(\text{LiMn}_2\text{O}_4/\text{CNT})//\text{AC}$ hybrid supercapacitor. The charge/discharge performance of the capacitor was tested using a LAND CT2001A autocyler (Wuhan, China) conducted at 30°C .

3. Results and discussion

3.1. Structural analysis by XRD and morphological observation by TEM

Fig. 1(a) shows the X-ray diffraction (XRD) patterns of the $\text{LiMn}_2\text{O}_4/\text{CNT}$ composite materials heat treated at 700°C for 0 h , 4.5 h , 8 h and 12 h , respectively, and the $\text{LiMn}_2\text{O}_4/\text{AC}$ composite material heat treated at 700°C for 8 h .

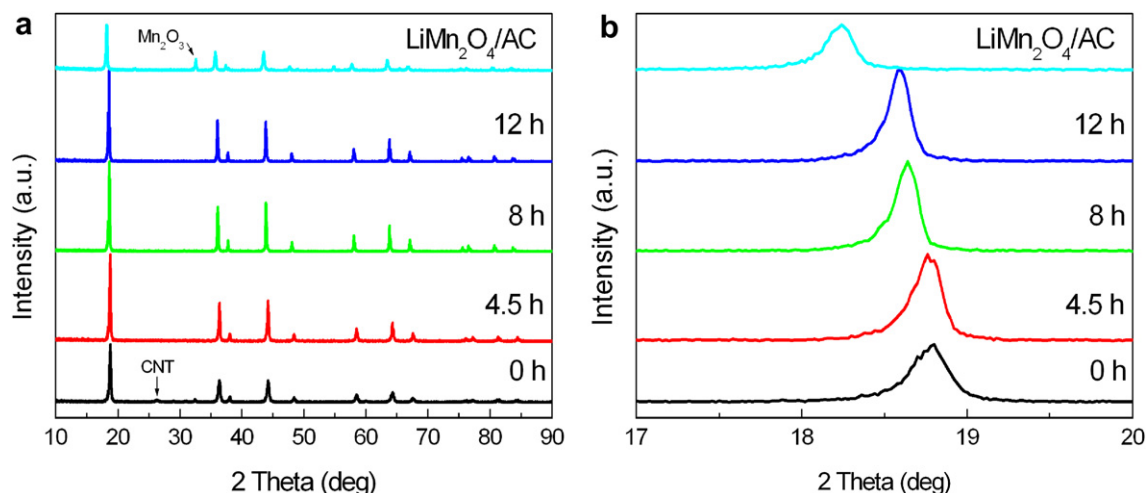
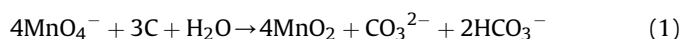


Fig. 1. (a) XRD patterns of $\text{LiMn}_2\text{O}_4/\text{CNT}$ composite materials heat treated at 700°C for 0 h , 4.5 h , 8 h and 12 h , respectively, and $\text{LiMn}_2\text{O}_4/\text{AC}$ composite material heat treated at 700°C for 8 h , and (b) close-up view around 18.5° .

Fig. 1(b) is the close-up view of Fig. 1(a) at 2θ angle around 18.5° . It can be seen from Fig. 1(a) that several reflections occur at ca. 18.6° , 36.2° , 37.7° , 44.0° , 48.1° , 58.1° , 64.0° , 67.6° , 76.0° , 77.0° , 81.0° and 84.0° , which correspond to the characteristic diffraction peaks of cubic spinel-type LiMn_2O_4 (PDF 35-0782, space group $Fd3m$). The as-synthesized $\text{LiMn}_2\text{O}_4/\text{CNT}$ composite material shows a weak reflection at ca. 26.2° that accords well with the characteristic diffraction peak for graphite carbon (PDF 75-2078), and hence, this reflection should be ascribed to the CNTs in the composite (for reference, the XRD pattern of the pure MWCNT is shown in Fig. S1 in the supporting information). After heat treatment, the intensities of the diffraction peaks of LiMn_2O_4 in the composites are increased, and on the contrary, the diffraction peak of CNTs disappeared. In addition, the diffraction peaks of LiMn_2O_4 shift toward small angle direction and the peak width narrow down gradually with increasing heat treatment time, as can be seen clearly in Fig. 1(b). These results suggest that the lattice constant and crystallinity of the LiMn_2O_4 increase with increasing heat treatment time. Compared with the $\text{LiMn}_2\text{O}_4/\text{CNT}$ material heat treated at 700°C for 8 h , the diffraction intensities of peaks for the $\text{LiMn}_2\text{O}_4/\text{AC}$ material heat treated under like conditions are obviously lower, and the peaks shift toward small angle direction. Besides, two additional weak diffraction peaks occur at ca. 32.5° and 55.0° , which correspond to the two stronger characteristic diffraction peaks of Mn_2O_3 (PDF 73-1826), indicating the presence of a small amount of Mn_2O_3 impurity in the material.

Fig. 2(a) shows the transmission electron microscope (TEM) image of the MnO_2/CNT nanocomposite precursor. As can be seen, numerous MnO_2 nanoflakes are self-assembled and closely wrap around the CNTs, forming uniform worm-like nanotubes with core-shell (CNT- MnO_2) hierarchical architecture (the TEM image of the MnO_2/CNT nanocomposite with a higher magnification is shown in Fig. S2, clearly showing the assembly of the nanoflakes). This is the result of in situ reduction of KMnO_4 at the surface of CNTs. XRD analysis result (Fig. S3) confirms that the formed MnO_2 in the MnO_2/CNT composite is layered K-birnessite-type MnO_2 (potassium manganese oxide hydrate) with monoclinic $C2/m$ (12) space group (PDF 80-1098). The stoichiometric reaction of KMnO_4 with CNT can be expressed as [52]:



The TEM image of the as-synthesized $\text{LiMn}_2\text{O}_4/\text{CNT}$ nanocomposite by hydrothermal reaction between MnO_2/CNT and LiOH

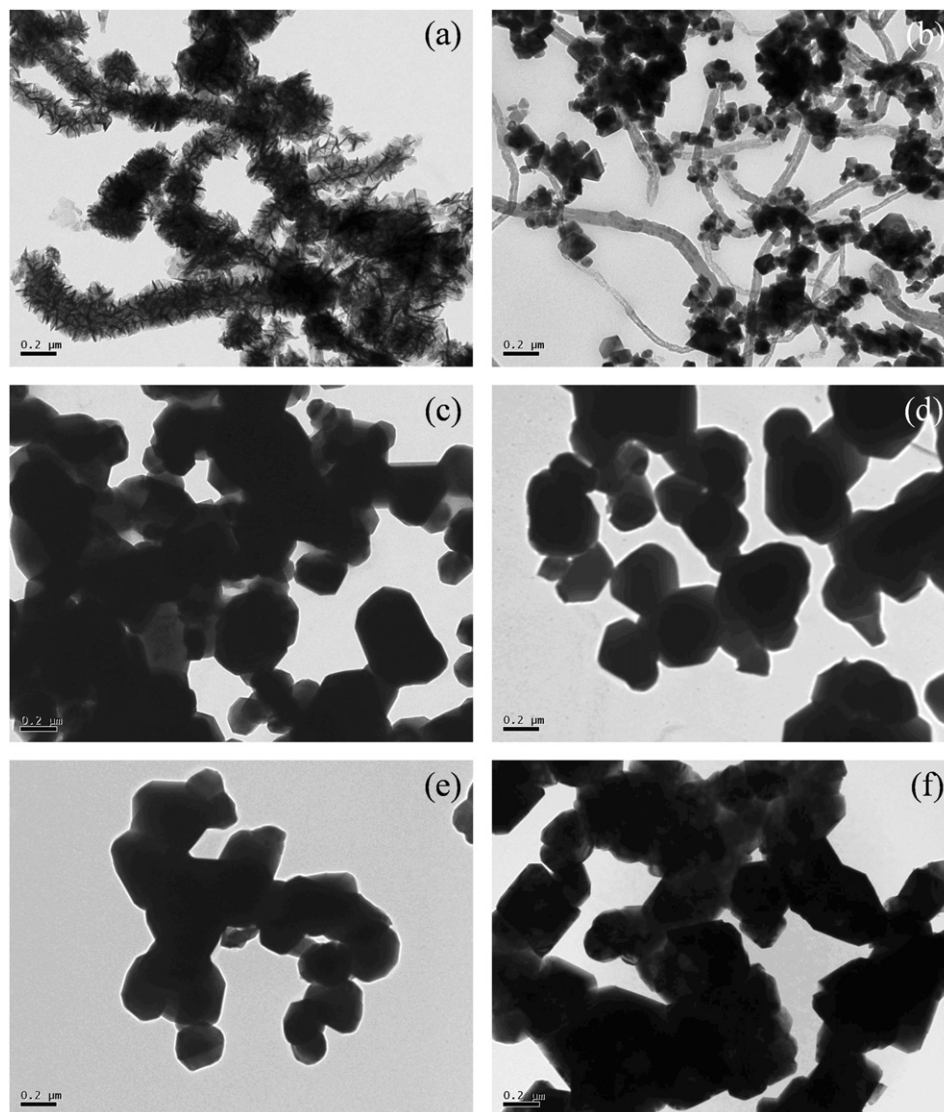
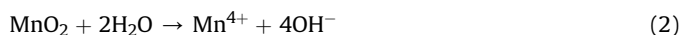


Fig. 2. TEM images of (a) MnO₂/CNT nanocomposite precursor, (b) as-synthesized LiMn₂O₄/CNT nanocomposite by hydrothermal reaction, (c, d, e) LiMn₂O₄/CNT after heat treatment for 4.5 h, 8 h and 12 h, respectively, and (f) LiMn₂O₄/AC after heat treatment for 8 h.

is shown in Fig. 2(b). As can be seen, after hydrothermal reaction, LiMn₂O₄ aggregates of nanocrystals are formed at the surface of CNTs. However, some naked segments of CNTs can be clearly observed, which is different from the case of the MnO₂/CNT precursor. This result suggests that the hydrothermal reaction between MnO₂ and LiOH solution would follow the dissolution–recrystallization mechanism [48]:



The thermogravimetric–differential thermal analysis (TG–DTA) curves of the as-synthesized LiMn₂O₄/CNT composite are displayed in Fig. S4. A strong exothermic peak can be observed at around 452 °C, corresponding to the quick weight loss around this temperature. This weight loss can be attributed to the oxidative combustion of CNTs existing in the as-synthesized LiMn₂O₄/CNT composite.

Fig. 2(c)–(e) shows the TEM images of the LiMn₂O₄/CNT composite materials after heat treatment at 700 °C for 4.5 h, 8 h and

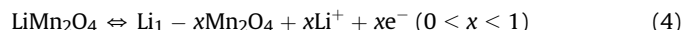
12 h, respectively. Compared with Fig. 2(b), the heat treated materials show the morphology of aggregates of LiMn₂O₄ crystallites with increased sizes (~150–400 nm), and no naked CNT segments could be observed because the naked CNT segments observed in Fig. 2(b) were oxidized by oxygen in air atmosphere. In order to know whether there are short CNT segments enwrapped in the heat treated LiMn₂O₄/CNT materials, a given amount of the LiMn₂O₄/CNT material heat treated at 700 °C for 12 h was dissolved by concentrated nitric acid. It is interesting that the LiMn₂O₄ was fully dissolved, but a very small amount of insoluble solid residua still remained in the solution. The solid residua were separated by centrifugal separation and then subjected to TEM observation. Fig. S5 shows the TEM images of the solid residua. As can be seen, two or three long CNT segments can be observed clearly in the TEM images, but the majority of the residual substance shows the morphology of aggregate of numerous very short CNT segments. On the other hand, the carbon content of the as-synthesized LiMn₂O₄/CNT and the LiMn₂O₄/CNT heat treated for 8 h and 12 h were determined to be 10.50 wt%, 0.107 wt% and 0.059 wt%, respectively, by elemental analysis (Table S1). Based on the above results, we can infer with reason that in the process of heat treatment, the well

enwrapped CNT segments (covered air-tightly by LiMn_2O_4 aggregates in the as-synthesized $\text{LiMn}_2\text{O}_4/\text{CNT}$) could not be oxidized (corresponding to the observed long CNT segments in Fig. S5), whereas the naked CNT segments (observed in Fig. 2(b)) would be fully oxidized. Besides, the numerous very short CNT segments (the majority of the residual substance shown in Fig. S5) should be originated from the CNT segments which are loosely covered (not covered air-tightly) by LiMn_2O_4 aggregates. The numerous unoxidized short CNT segments are enwrapped in the composite material and would act as the inner electric micro-conductors upon charging and discharging of the composite electrode material.

Fig. 2(f) shows the TEM image of the $\text{LiMn}_2\text{O}_4/\text{AC}$ composite material heat treated at 700°C for 8 h. As can be seen, it also shows the morphology of aggregates of LiMn_2O_4 crystals which is similar to that shown in Fig. 2(d). The TEM images of its precursor, i.e., the MnO_2/AC composite are shown in Fig. S6. It can be seen from Fig. S6 that numerous MnO_2 nanowires are formed at the surface of the activated carbon and some of them are self-assembled to echinus-like architecture. The TEM image of the as-synthesized $\text{LiMn}_2\text{O}_4/\text{AC}$ composite by hydrothermal reaction between MnO_2/AC composite and LiOH is shown in Fig. S7. Its carbon content before and after heat treatment is 21.46 wt% and 0.273 wt%, respectively (Table S1).

3.2. Influence of heat treatment time on electrochemical performance of $\text{LiMn}_2\text{O}_4/\text{CNT}$ composite

Fig. 3 shows the cyclic voltammograms (CVs) of the $\text{LiMn}_2\text{O}_4/\text{CNT}$ composite before and after heat treatment for different periods of time recorded at a scan rate of 1 mV s^{-1} . The responsive current was calculated based on the mass of the $\text{LiMn}_2\text{O}_4/\text{CNT}$ composite material. As can be seen, two pairs of reversible redox peaks can be observed between 0.6 and 1.2 V (vs. SCE), which correspond to the characteristic intercalation/deintercalation peaks of LiMn_2O_4 in 4 V (vs. Li^+/Li) level in a nonaqueous organic electrolyte corresponding to the following reaction:



where, the lower-potential redox peaks correspond to Li^+ extraction and insertion over the x value range of $0 \leq x \leq 0.5$ in $\text{Li}_x\text{Mn}_2\text{O}_4$, and the higher-potential redox peaks correspond to Li^+ extraction and insertion over the x value range of $0.5 \leq x \leq 1$ [6].

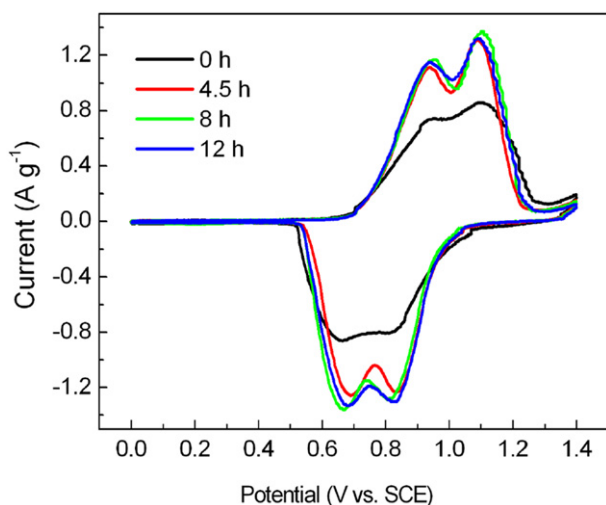


Fig. 3. CVs of $\text{LiMn}_2\text{O}_4/\text{CNT}$ composite before and after heat treatment for different periods of time at a scan rate of 1 mV s^{-1} .

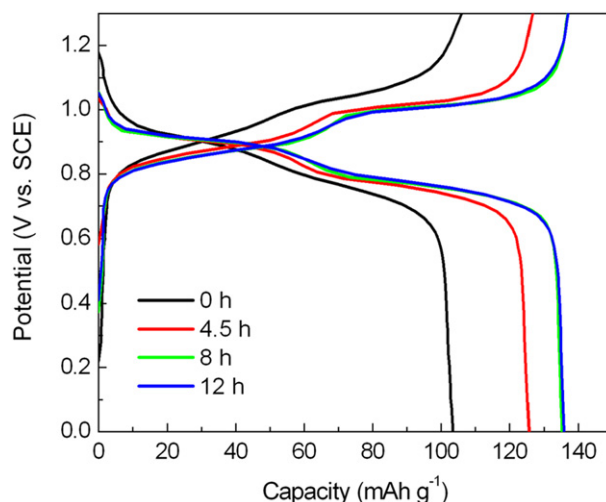


Fig. 4. Charge–discharge curves of $\text{LiMn}_2\text{O}_4/\text{CNT}$ composite before and after heat treatment for different periods of time at a current rate of 500 mA g^{-1} .

After heat treatment, the redox peaks become sharp and clear. In addition, both the peak current and the encircled area of the CV curve are all increased markedly, suggesting the improved electrochemical activity and specific capacity. This result is because that the crystallinity and lattice constant of the LiMn_2O_4 in the composite are increased after heat treatment (Fig. 1), and hence its electrochemical activity is also increased significantly. The peak current and the encircled area of the CV curve for the $\text{LiMn}_2\text{O}_4/\text{CNT}$ composite heat treated for 8 h are close to those of the one heat treated for 12 h, and are a little larger than those of the one heat treated for 4.5 h.

The charge–discharge curves of the $\text{LiMn}_2\text{O}_4/\text{CNT}$ composite before and after heat treatment for different periods of time at a current rate of 500 mA g^{-1} are shown in Fig. 4. It can be seen that the charge and discharge curves present two potential plateaus corresponding to the two pairs of redox peaks observed in the CVs (Fig. 3). The charge and discharge curves of the $\text{LiMn}_2\text{O}_4/\text{CNT}$ composite heat treated for 8 h are almost identical with those of the one heat treated for 12 h, showing a high specific capacity of 136 mAh g^{-1} which is higher than that of the one heat treated for

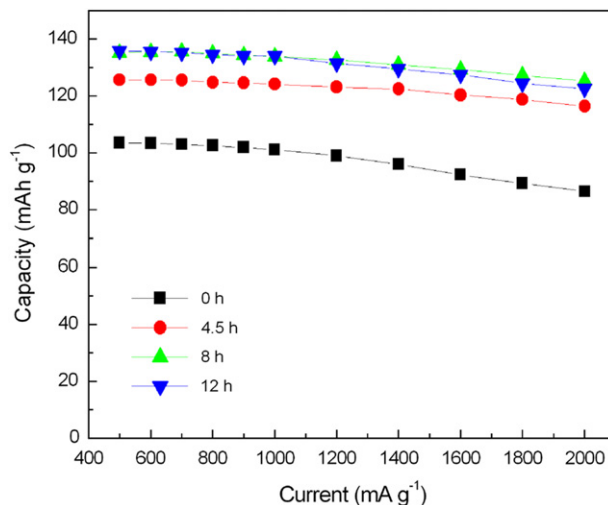


Fig. 5. Rate capability of $\text{LiMn}_2\text{O}_4/\text{CNT}$ composite before and after heat treatment for different periods of time.

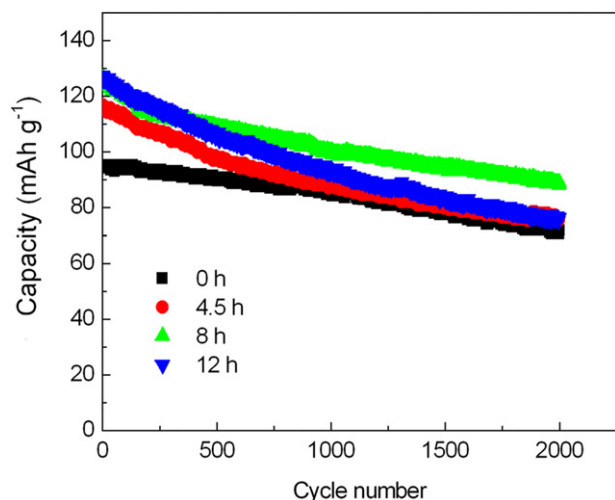


Fig. 6. Cycle performance of LiMn₂O₄/CNT composite before and after heat treatment for different periods of time at a charge/discharge current rate of 2000 mA g⁻¹.

4.5 h (126 mAh g⁻¹). However, the as-synthesized LiMn₂O₄/CNT (without heat treatment) exhibits the lowest specific capacity (only 103 mAh g⁻¹). These results are consistent with the CV results observed in Fig. 3. Nevertheless, only in consideration of the net

LiMn₂O₄ active material contained in the as-synthesized LiMn₂O₄/CNT composite, the specific capacity of the net LiMn₂O₄ is calculated to be ca. 115 mAh g⁻¹, which is still lower than that of the heat treated materials.

Fig. 5 shows the specific discharge capacities of the LiMn₂O₄/CNT composite before and after heat treatment for different periods of time at different charge/discharge rates. When the current is increased from 500 (~3.4 C) to 2000 mA g⁻¹ (~13.5 C), the specific capacities of the LiMn₂O₄/CNT composite before and after heat treatment for 4.5 h, 8 h and 12 h are decreased from 103.5, 125.6, 135.1 and 135.8 mAh g⁻¹ to 86.4, 116.4, 125.3 and 122.5 mAh g⁻¹, i.e., decreased by 16.5%, 7.3%, 7.2% and 9.8%, respectively. The rate charge/discharge performances follow the order of 8 h, ≈ 4.5 h, 12 h, 0 h. These results suggest that post heat treatment has not only a significant positive influence on specific capacity but also a positive influence on rate capability of the LiMn₂O₄/CNT composite material.

Fig. 6 shows the cycling performance of the LiMn₂O₄/CNT composite before and after heat treatment for different periods of time at a high charge/discharge current rate of 2000 mA g⁻¹. After 2000 cycles, the discharge specific capacities of the LiMn₂O₄/CNT composite before and after heat treatment for 4.5 h, 8 h and 12 h are decreased from 95.2, 116.9, 126.4 and 127.5 mAh g⁻¹ to 71.8, 75.7, 88.6 and 76.3 mAh g⁻¹, corresponding to the capacity retentions of 75.4%, 64.8%, 70.1% and 59.8%, respectively. After heat treatment, the initial specific capacity of the LiMn₂O₄/CNT composite is

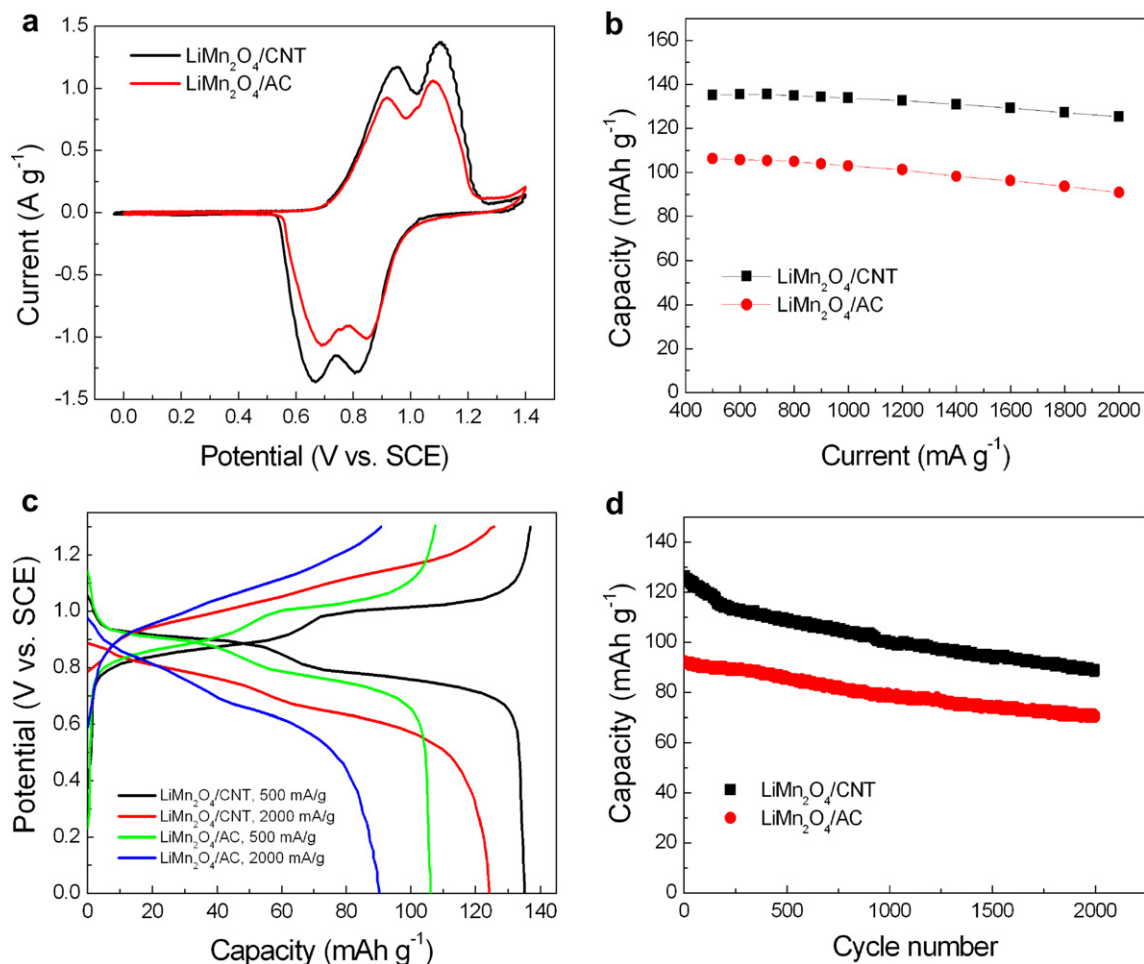


Fig. 7. (a) CVs recorded at a scan rate of 1 mV s⁻¹, (b) rate capability, (c) charge and discharge curves at current rates of 500 and 2000 mA g⁻¹, and (d) cycling performance at a current rate of 2000 mA g⁻¹ for LiMn₂O₄/CNT and LiMn₂O₄/AC composites heat treated at 700 °C for 8 h.

obviously increased, and in general increases with increasing heat treatment time. The $\text{LiMn}_2\text{O}_4/\text{CNT}$ composite heat treated for 8 h shows an initial specific capacity close to, but a better cycling stability than that heat treated for 12 h. After 2000 cycles, the specific capacity of the $\text{LiMn}_2\text{O}_4/\text{CNT}$ composite heat treated for 8 h is obviously higher than that of the others. In conclusion, the $\text{LiMn}_2\text{O}_4/\text{CNT}$ composite heat treated for 8 h presents not only a larger high-rate initial specific capacity, but also a better cycling stability.

3.3. Comparison of electrochemical performance for $\text{LiMn}_2\text{O}_4/\text{CNT}$ composite and LiMn_2O_4 heat treated at 700°C for 8 h

Fig. 7(a) shows the CVs of the $\text{LiMn}_2\text{O}_4/\text{CNT}$ and $\text{LiMn}_2\text{O}_4/\text{AC}$ composites heat treated at 700°C for 8 h at a scan rate of 1 mV s^{-1} in 5 M LiNO_3 aqueous electrolyte. As can be seen, the peak currents of the $\text{LiMn}_2\text{O}_4/\text{CNT}$ electrode are obviously higher than those of the $\text{LiMn}_2\text{O}_4/\text{AC}$ electrode. Fig. 7(b) shows the rate capability of the $\text{LiMn}_2\text{O}_4/\text{CNT}$ electrode in comparison with the $\text{LiMn}_2\text{O}_4/\text{AC}$ electrodes. The specific discharge capacity of the $\text{LiMn}_2\text{O}_4/\text{CNT}$ electrode at any a current rate is obviously higher than that of the $\text{LiMn}_2\text{O}_4/\text{AC}$ electrode. When the current rate is increased from 500 to 2000 mA g^{-1} , the specific capacities of the $\text{LiMn}_2\text{O}_4/\text{CNT}$ and $\text{LiMn}_2\text{O}_4/\text{AC}$ electrodes are decreased by 7.3% and 14.5%, respectively. The presented specific capacity and rate capability of the

heat treated $\text{LiMn}_2\text{O}_4/\text{CNT}$ composite electrode in this work are obviously superior to those of the reported $\text{LiMn}_2\text{O}_4/\text{conductive carbon composite electrodes}$ either in the nonaqueous electrolytes [47,48,50–52] or in an aqueous electrolyte [49]. Up to now, the high specific capacity of 126 mAh g^{-1} obtained in the present work is the highest for LiMn_2O_4 -based materials at the high current of 2 A g^{-1} ($\sim 13.5^\circ\text{C}$), as far as we know. The typical charge/discharge curves of the $\text{LiMn}_2\text{O}_4/\text{CNT}$ and $\text{LiMn}_2\text{O}_4/\text{AC}$ electrodes at the current densities of 500 and 2000 mA g^{-1} are shown in Fig. 7(c). It can be seen that the charge potential of the $\text{LiMn}_2\text{O}_4/\text{CNT}$ electrode is lower than that of the $\text{LiMn}_2\text{O}_4/\text{AC}$ electrode and the discharge potential of the $\text{LiMn}_2\text{O}_4/\text{CNT}$ electrode is higher than that of the $\text{LiMn}_2\text{O}_4/\text{AC}$ electrode at a same current density. The above results demonstrate that the $\text{LiMn}_2\text{O}_4/\text{CNT}$ electrode can exhibit not only higher specific capacity and higher discharge potential, but also excellent high-rate capability. The high specific capacity and excellent high-rate capability can be attributed to the enhancement in electron transfer within the LiMn_2O_4 caused by the small amount of enwrapped CNT segments and the increase in crystallinity of LiMn_2O_4 caused by the post heat treatment. The charge/discharge curves of the $\text{LiMn}_2\text{O}_4/\text{CNT}$ after heat treatment for 8 h at different current rates are shown in Fig. S8.

Fig. 7(d) shows the cycling performance of the $\text{LiMn}_2\text{O}_4/\text{CNT}$ and $\text{LiMn}_2\text{O}_4/\text{AC}$ electrodes at the current of 2000 mA g^{-1} over the potential window of 0–1.3 V (SCE). As can be seen, the capacity of

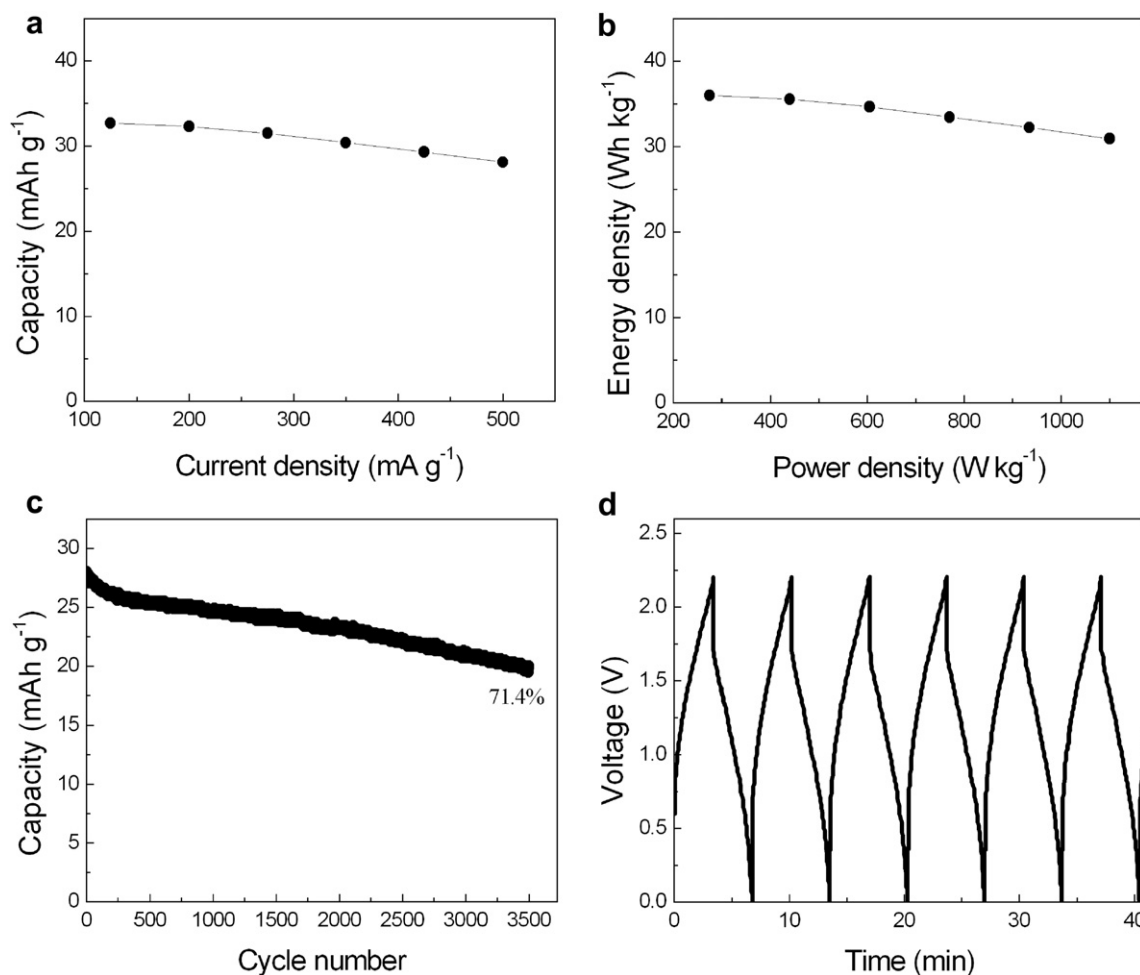


Fig. 8. (a) Rate charge/discharge capability, (b) Ragone plot, (c) cycle performance and (d) initial repeated charge/discharge profile at a current rate of 500 mA g^{-1} for ($\text{LiMn}_2\text{O}_4/\text{CNT}$)/AC hybrid supercapacitor.

the $\text{LiMn}_2\text{O}_4/\text{CNT}$ electrode is always higher than that of the $\text{LiMn}_2\text{O}_4/\text{AC}$ electrode through the completed 2000 cycles. The charge/discharge profile for the initial 6 cycles of the $\text{LiMn}_2\text{O}_4/\text{CNT}$ heat treated for 8 h at 2000 mA g^{-1} is shown in Fig. S9, and the selected charge/discharge curves for the 1st, 1000th and 2000th cycles are shown in Fig. S10. The heat treated $\text{LiMn}_2\text{O}_4/\text{CNT}$ composite electrode exhibits a pseudocapacitive behavior with a high initial specific capacity of ca. 126 mAh g^{-1} , corresponding to a high average specific capacitance of 349 F g^{-1} in the operating potential window. Therefore, this composite material was employed to fabricate the positive electrode for the $(\text{LiMn}_2\text{O}_4/\text{CNT})//\text{AC}$ hybrid supercapacitor for further study.

3.4. Charge–discharge performance of $(\text{LiMn}_2\text{O}_4/\text{CNT})//\text{AC}$ supercapacitor

Fig. 8(a)–(d) shows the rate charge/discharge capability, energy density versus power density (Ragone plot), cycle performance and initial repeated charge/discharge profile at a current rate of 500 mA g^{-1} for the $(\text{LiMn}_2\text{O}_4/\text{CNT})//\text{AC}$ hybrid supercapacitor. The current density, specific capacity, energy density and power density of the capacitor were calculated based on the total mass of the positive and negative active materials. The mass ratio of the positive active material ($\text{LiMn}_2\text{O}_4/\text{CNT}$) to the negative active material (AC) is 1:3 in consideration of the respective specific capacities of the two electrodes. We can see from Fig. 8(a) that at the lower current rate of 125 mA g^{-1} (corresponding to 500 mA g^{-1} for the positive electrode and 167 mA g^{-1} for the negative electrode, respectively), the specific capacity of the capacitor is 32.7 mAh g^{-1} , which is about one quarter of the specific capacity of the single $\text{LiMn}_2\text{O}_4/\text{CNT}$ electrode at 500 mA g^{-1} . At the higher current rate of 500 mA g^{-1} (corresponding to 2000 mA g^{-1} for the positive electrode and 667 mA g^{-1} for the negative electrode, respectively), the specific capacity of the capacitor is 28.1 mAh g^{-1} , which is a little less than one quarter of the specific capacity of the single $\text{LiMn}_2\text{O}_4/\text{CNT}$ electrode at 2000 mA g^{-1} . That is to say, the rate capability of the $(\text{LiMn}_2\text{O}_4/\text{CNT})//\text{AC}$ capacitor is only a little inferior to that of the single $\text{LiMn}_2\text{O}_4/\text{CNT}$ electrode, owing to the inferior rate capability of the AC negative electrode used in the capacitor.

However, the capacitor presents a good energy density versus power density characteristic which can be seen in Fig. 8(b). When the power density is 275 W kg^{-1} , the energy density is 36 Wh kg^{-1} . When the power density is increased to 1100 W kg^{-1} , the energy density is still as high as 31 Wh kg^{-1} , indicating an excellent high-power charge/discharge capability. The excellent high-power capability should be attributed to the excellent rate capability of the $\text{LiMn}_2\text{O}_4/\text{CNT}$ cathode and the high operating voltage of the capacitor.

We can see from Fig. 8(c) that the capacitor can also exhibit a good charge/discharge cycle performance at the high-rate of 500 mA g^{-1} with a capacity retention of 71.4% after 3500 cycles. Fig. 8(d) shows the corresponding charge/discharge curves for the initial 6 cycles. As can be seen, the capacitor displays a capacitive behavior at this high current rate, and a full charge/discharge cycle can be completed within a short time of 7 min. The selected charge/discharge curves for the 1st, 2000th and 3500th cycles are shown in Fig. S11.

4. Conclusions

In this paper, the $\text{LiMn}_2\text{O}_4/\text{CNT}$ composite was prepared by a two-step procedure, i.e., by in situ redox reaction between KMnO_4 and MWCNTs to obtain MnO_2/CNT precursor followed by hydrothermal reaction between the MnO_2/CNT composite and LiOH solution to obtain $\text{LiMn}_2\text{O}_4/\text{CNT}$ composite. After heat treatment at

700°C in air atmosphere, the majority of the CNT segments in the as-synthesized $\text{LiMn}_2\text{O}_4/\text{CNT}$ composite are oxidized except for a small amount of remaining very short CNT segments, and hence a composite material consist of LiMn_2O_4 and enwrapped segmented carbon nanotubes was obtained. The $\text{LiMn}_2\text{O}_4/\text{CNT}$ composite material heat treated at 700°C for 8 h presented high specific capacity (136 mAh g^{-1} at the current density of 500 mA g^{-1}) and excellent rate capability (126 mAh g^{-1} at the current density of 2000 mA g^{-1}) in 5 M LiNO_3 aqueous electrolyte, which are much superior to those of the as-synthesized $\text{LiMn}_2\text{O}_4/\text{CNT}$ composite. Besides, the $(\text{LiMn}_2\text{O}_4/\text{CNT})/5 \text{ M LiNO}_3/\text{AC}$ hybrid supercapacitor with this composite as the cathode material presented excellent high-power capability and good cycling stability.

It can be concluded that the post heat treatment and the enwrapped CNT segments have significant positive effects on the performance of the LiMn_2O_4 -based material. Firstly, heat treatment at a higher temperature can increase the electrochemical activity and hence the utilization rate of LiMn_2O_4 active material. Secondly, although the majority of the CNT segments in the as-synthesized $\text{LiMn}_2\text{O}_4/\text{CNT}$ composite are oxidized during the heat treatment process, the remaining enwrapped short CNT segments in the composite can act as the inner electric micro-conductors upon charging and discharging of the composite material. This effect can not only increase the utilization rate of LiMn_2O_4 active material (or specific capacity) at a lower current density, but also significantly increase the specific capacity at a high current density. This high-performance $\text{LiMn}_2\text{O}_4/\text{CNT}$ composite would be a promising cathode material for high-power energy storage devices. In addition, this unique architecture of $\text{LiMn}_2\text{O}_4/\text{CNT}$ composite and its preparation method would be applied to other metal oxide/CNT composite electrode materials with fascinating electrochemical performance.

Acknowledgments

This work was supported by Leading Academic Discipline Project of Shanghai Municipal Education Commission (Project Number: J50102). Instrumental Analysis & Research Center of Shanghai University is gratefully acknowledged for XRD and TEM experiments.

Appendix A. Supplementary material

Supplementary material associated with this article can be found, in the online version, at <http://dx.doi.org/10.1016/j.jpowsour.2013.01.182>.

References

- [1] S. Nieto, S.B. Majumder, R.S. Katiyar, J. Power Sources 136 (2004) 88.
- [2] T. Kakuda, K. Uematsu, K. Toda, M. Sato, J. Power Sources 167 (2007) 499.
- [3] R.S. Liu, C.H. Shen, Solid State Ionics 157 (2003) 95.
- [4] R. Thirunakaran, K.T. Kim, Y.M. Kang, C.Y. Seo, J. Young-Lee, J. Power Sources 137 (2004) 100.
- [5] W. Li, J.R. Dahn, D.S. Wainwright, Science 264 (1994) 1115.
- [6] N.C. Li, C.J. Patrissi, G.L. Che, C.R. Martin, J. Electrochem. Soc. 147 (2000) 2044.
- [7] A. Eftekhari, Electrochim. Acta 47 (2001) 495.
- [8] T. Grygar, P. Bezdička, P. Piszora, J. Solid State Electrochem. 5 (2001) 487.
- [9] M. Jayalakshmi, M.M. Rao, F. Scholz, Langmuir 19 (2003) 8403.
- [10] J.W. Lee, S.I. Pyun, Electrochim. Acta 49 (2004) 753.
- [11] G.J. Wang, H.P. Zhang, L.J. Fu, B. Wang, Y.P. Wu, Electrochem. Commun. 9 (2007) 1873.
- [12] N. Nakayama, T. Nozawa, Y. Iriyama, T. Abe, Z. Ogumi, K. Kikuchi, J. Power Sources 174 (2007) 695.
- [13] N. Cvjetanin, I. Stojkovic, M. Mitric, S. Mentus, J. Power Sources 174 (2007) 1117.
- [14] J.Y. Luo, Y.Y. Xia, Adv. Funct. Mater. 17 (2007) 3877.
- [15] H.B. Wang, Y.Q. Zeng, K.L. Huang, S.Q. Liu, L.Q. Chen, Electrochim. Acta 52 (2007) 5102.

- [16] D. Tonti, M.J. Torralvo, E. Enciso, I. Sobrados, J. Sanz, *Chem. Mater.* 20 (2008) 4783.
- [17] P. He, J.Y. Luo, J.X. He, Y.Y. Xia, *J. Electrochem. Soc.* 156 (2009) A209.
- [18] K. Katakura, K. Wada, Y. Kajiki, A. Yamamoto, Z. Ogumi, *J. Power Sources* 189 (2009) 240.
- [19] N. Nakayama, I. Yamada, Y. Huang, T. Nozawa, Y. Iriyama, T. Abe, Z. Ogumi, *Electrochim. Acta* 54 (2009) 3428.
- [20] L. Tian, A.B. Yuan, *J. Power Sources* 192 (2009) 693.
- [21] I.B. Stojković, N.D. Cvjetičanin, S.V. Mentus, *Electrochem. Commun.* 12 (2010) 371.
- [22] Y.P. Lin, N.L. Wu, *J. Power Sources* 196 (2011) 851.
- [23] M.S. Zhao, Q.Y. Zheng, F. Wang, W.M. Dai, X.P. Song, *Electrochim. Acta* 56 (2011) 3781.
- [24] M.S. Zhao, X.P. Song, F. Wang, W.M. Dai, X.G. Lu, *Electrochim. Acta* 56 (2011) 5673.
- [25] H. Manjunatha, K.C. Mahesh, G.S. Suresh, T.V. Venkatesha, *Electrochim. Acta* 56 (2011) 1439.
- [26] W. Tang, S. Tian, L.L. Liu, L. Li, H.P. Zhang, Y.B. Yue, Y. Bai, Y.P. Wu, K. Zhu, *Electrochem. Commun.* 13 (2011) 205.
- [27] Q.T. Qu, L.J. Fu, X.Y. Zhan, D. Samuelis, J. Maier, L. Li, S. Tian, Z.H. Li, Y.P. Wu, *Energy Environ. Sci.* 4 (2011) 3985.
- [28] G.J. Wang, N.H. Zhao, L.C. Yang, Y.P. Wu, H.Q. Wu, R. Holze, *Electrochim. Acta* 52 (2007) 4911.
- [29] R. Ruffo, C. Wessells, R.A. Huggins, Y. Cui, *Electrochem. Commun.* 11 (2009) 247.
- [30] G.J. Wang, Q.T. Qu, B. Wang, Y. Shi, S. Tian, Y.P. Wu, R. Holze, *Electrochim. Acta* 54 (2009) 1199.
- [31] M.M. Rao, M. Jayalakshmi, O. Schäf, U. Guth, H. Wulff, F. Scholz, *J. Solid State Electrochem.* 4 (1999) 17.
- [32] G.J. Wang, L.J. Fu, B. Wang, N.H. Zhao, Y.P. Wu, R. Holze, *J. Appl. Electrochem.* 38 (2008) 579.
- [33] Y.Q. Zhao, G.Q. Zhang, H.L. Li, *Solid State Ionics* 177 (2006) 1335.
- [34] C.H. Mi, X.G. Zhang, H.L. Li, *J. Electroanal. Chem.* 602 (2007) 245.
- [35] P. He, J.L. Liu, W.J. Cui, J.Y. Luo, Y.Y. Xia, *Electrochim. Acta* 56 (2011) 2351.
- [36] J. Köhler, H. Makihara, H. Uegaito, H. Inoue, M. Toki, *Electrochim. Acta* 46 (2000) 59.
- [37] G.J. Wang, Q.T. Qu, B. Wang, Y. Shi, S. Tian, Y.P. Wu, R. Holze, *J. Power Sources* 189 (2009) 503.
- [38] A. Caballero, J. Morales, O.A. Vargas, *J. Power Sources* 195 (2010) 4318.
- [39] X.H. Liu, T. Saito, T. Doi, S. Okada, J. Yamaki, *J. Power Sources* 189 (2009) 706.
- [40] S.D. Zhang, Y.M. Li, C.Z. Wu, F. Zheng, Y. Xie, *J. Phys. Chem. C* 113 (2009) 15058.
- [41] I. Stojković, N. Cvjetičanin, I. Pašti, M. Mitrić, S. Mentus, *Electrochem. Commun.* 11 (2009) 1512.
- [42] A.B. Yuan, L. Tian, W.M. Xu, Y.Q. Wang, *J. Power Sources* 195 (2010) 5032.
- [43] W.M. Xu, A.B. Yuan, L. Tian, Y.Q. Wang, *J. Appl. Electrochem.* 41 (2011) 453.
- [44] J.Y. Luo, Y.G. Wang, H.M. Xiong, Y.Y. Xia, *Chem. Mater.* 19 (2007) 4791.
- [45] Y.L. Ding, X.B. Zhao, J. Xie, G.S. Cao, T.J. Zhu, H.M. Yu, C.Y. Sun, *J. Mater. Chem.* 21 (2011) 9475.
- [46] Y.M. Wu, Z.H. Wen, H.B. Feng, J.H. Li, *Small* 8 (2012) 858.
- [47] T.J. Patey, R. Büchel, S.H. Ng, F. Krumeich, S.E. Pratsinis, P. Novák, *J. Power Sources* 189 (2009) 149.
- [48] S.B. Ma, K.W. Nam, W.S. Yoon, S.M. Bak, X.Q. Yang, B.W. Cho, K.B. Kim, *Electrochem. Commun.* 11 (2009) 1575.
- [49] S.Y. Chen, C.H. Mi, L.H. Su, B. Gao, Q.B. Fu, X.G. Zhang, *J. Appl. Electrochem.* 39 (2009) 1943.
- [50] H.J. Yue, X.K. Huang, D.P. Lv, Y. Yang, *Electrochim. Acta* 54 (2009) 5363.
- [51] X.M. Liu, Z.D. Huang, S. Oh, P.C. Ma, P.C.H. Chan, G.K. Vedam, K. Kang, J.K. Kim, *J. Power Sources* 195 (2010) 4290.
- [52] X.L. Jia, C.Z. Yan, Z. Chen, R.R. Wang, Q. Zhang, L. Guo, F. Wei, Y.F. Lu, *Chem. Commun.* 47 (2011) 9669.
- [53] Y.Y. Liu, C.B. Cao, *Electrochim. Acta* 55 (2010) 4694.
- [54] F.F. Pan, X.Y. Chen, H.J. Li, X.D. Xin, Q.Q. Chang, K.N. Jiang, W.L. Wang, *Electrochem. Commun.* 13 (2011) 726.
- [55] A. Vu, A. Stein, *Chem. Mater.* 23 (2011) 3237.